

# **Studying the adsorption of emerging organic contaminants in zeolites with dispersion-corrected density functional theory calculations: From numbers to recommendations**

***Michael Fischer***

Crystallography and Geomaterials, Faculty of Geosciences, University of Bremen, Klagenfurter Straße 2-4, 28359 Bremen, Germany

Bremen Center for Computational Materials Science, University of Bremen, 28359 Bremen, Germany

MAPEX Center for Materials and Processes, University of Bremen, 28359 Bremen, Germany

E-Mail: michael.fischer@uni-bremen.de

## **ABSTRACT**

It has been established that adsorption energies obtained from dispersion-corrected density functional theory (DFT) calculations show a considerable dependence on the choice of exchange-correlation functional and dispersion correction. A number of investigations have employed different approaches to compute adsorption energies of small molecules like methane, ethane, or carbon dioxide in different types of zeolites (all-silica, protonated, cation-exchanged), using reference values from high-level calculations and/or experiments. Such comparative studies are lacking for the adsorption of larger functional organic molecules such as pharmaceuticals or personal care products in zeolites, despite the potential relevance for various applications, among them contaminant removal and drug delivery. The present study aims to fill this gap by comparing adsorption energies and, for selected cases, equilibrium structures of adsorption complexes of emerging organic contaminants in all-silica zeolites, employing a total of 13 dispersion-corrected DFT approaches. Methods using a pairwise (D3) dispersion correction as well as non-local van der Waals density functionals were included. A comparison of adsorption energies obtained for a variety of emerging organic contaminants in zeolites with the MOR and FAU topologies showed that the absolute values vary widely, whereas the qualitative trend across the set of zeolite-contaminant combinations are not strongly dependent on the choice of functional. For a few cluster models, DFT adsorption energies were compared to reference values obtained with the random phase approximation. When combining these results with observations of previous benchmarking studies, the revvdW-DF2 and PBE-D3 functionals emerge as approaches that should be (relatively) free from a systematic tendency to deliver too negative adsorption energies.

## INTRODUCTION

The adsorption of functional organic molecules, such as pharmaceuticals, personal care products, herbicides, insecticides, etc., in high-silica and all-silica zeolites is relevant in the context of different applications: On the one hand, these hydrophobic adsorbents could be employed in the removal of emerging organic contaminants from wastewaters.<sup>[1]</sup> Promising results have been obtained, for example, for the use of faujasite-type zeolite Y (FAU framework<sup>[2]</sup>) to remove sulfonamide antibiotics<sup>[3,4]</sup> or other drugs like carbamazepine,<sup>[5]</sup> for high-silica mordenite (MOR framework) as adsorbent for various pharmaceuticals and other organic contaminants,<sup>[6,7]</sup> and for zeolite beta (BEA framework) in the removal of drugs,<sup>[8]</sup> pesticides,<sup>[9]</sup> and perfluoroalkyl substances.<sup>[10]</sup> On the other hand, high/all-silica zeolites could also find use as carrier materials in the controlled delivery of drug molecules<sup>[11–14]</sup> or for the encapsulation of organic UV filters, enhancing their UV filtering activity while at the same time preventing undesired release into the environment.<sup>[15]</sup> Further potential applications of zeolites involving the adsorption of sizeable organic molecules from the liquid phase include the recovery of valuable fractions from complex mixtures, *e.g.*, in the processing of rapeseed,<sup>[16]</sup> and the use of zeolites as solid sorbents in (micro)extraction.<sup>[17]</sup>

Given the vast number of potentially interesting organic species, and the multitude of zeolite frameworks that are available in highly or purely siliceous form (about 70 zeolite frameworks have been synthesised as all-silica zeolites to date<sup>[2,18]</sup>), it is clear that experimental investigations of the adsorption properties are feasible only for a small fraction of the theoretically possible adsorbent-guest combinations. To narrow down the selection, atomistic simulations can be employed to gauge the affinity of different zeolites towards a species of interest. Recent work showed a good correlation between zeolite-guest interaction energies and experimentally observed removal efficiencies for 21 organic contaminants in MOR- and FAU-type zeolites.<sup>[19]</sup> The interaction energies were computed using a very simplistic approach based on Monte Carlo (MC) simulations and subsequent energy minimisations with the DREIDING force field (FF),<sup>[20]</sup> indicating that even relatively crude simulations could be very useful to identify adsorbent-guest combinations of interest. Other authors have employed FF-based molecular dynamics (MD) simulations to study the diffusion of pharmaceuticals through zeolite structures in the context of drug delivery investigations.<sup>[12–14]</sup>

A crucial aspect in this regard is the suitability of the force field parameters to represent the relevant interatomic interactions in the system, especially the interactions between zeolite host and adsorbed molecules. For gas phase adsorption, a validation against experimental adsorption data is relatively straightforward, and high-quality FFs that accurately reproduce adsorption isotherms for gases like CO<sub>2</sub>, CH<sub>4</sub>, N<sub>2</sub>, or O<sub>2</sub> in all-silica zeolites have been developed.<sup>[21–24]</sup> For larger organics that are adsorbed from the liquid phase, the situation is

more complex, as a direct comparison to liquid-phase adsorption isotherms does not only require a reasonably accurate description of the interactions between zeolite and organic guest, but also of interactions between the organic species and the solvent (typically water). Some progress in this direction has been made, and expanded-ensemble MC simulations have been shown to reproduce liquid-phase adsorption data rather well.<sup>[25,26]</sup> Altogether, however, a validation against experimental data remains a very complex endeavour, not least due to the impact of structural defects (usually ignored in the simulations) on the experimental isotherms.

An alternative approach is the validation of FF parameters against electronic structure calculations, which can also be employed for cases where no experimental adsorption data are (yet) available. Moreover, an analysis of the results obtained at a higher level of theory can provide insights into the nature of the host-guest interactions. Given its good scaling behaviour and efficient implementation for periodic systems, density functional theory (DFT) is the most widely applicable electronic structure method for these systems. Due to the well-known shortcomings of standard DFT in describing long-range dispersion interactions, which play an important role for adsorption phenomena, recent investigations have usually employed dispersion-corrected “flavours” of DFT. For example, the DREIDING calculations carried out in one of the aforementioned studies<sup>[19]</sup> were supplemented by DFT calculations using the Perdew-Burke-Ernzerhof (PBE)<sup>[27]</sup> functional with a D3 dispersion correction<sup>[28]</sup> functional for selected systems. It was shown that FF and DFT give, by and large, the same trends, validating the conclusions drawn from the DREIDING calculations. A more comprehensive benchmarking was carried out by Schwalbe-Koda and Gómez-Bombarelli, who compared binding energies obtained from static and dynamic DREIDING calculations to reference values from DFT optimisations and DFT-based MD simulations using the PBE-D3 functional, considering a total of 227 combinations of zeolites and organic structure-directing agents (OSDAs).<sup>[29]</sup> Pointing out that the PBE-D3 functional has a tendency to overbind guest molecules (see below), they noted that it provides a good balance between accuracy and computational cost compared to more sophisticated approaches. Altogether, they observed a good correlation between FF and DFT calculations, especially when using the “frozen-pose” method to compute the DREIDING binding energies (calculation of the host-guest binding energy without relaxation of zeolite and OSDA). They proposed this method for large-scale FF-based screening studies of zeolite-OSDA pairs.

It is well established that DFT interaction energies show a strong dependence on the choice of exchange-correlation (XC) functional, which governs the description of short-range interactions, and (if included) the method to include long-range dispersion interactions. As a large variety of XC functionals and dispersion correction schemes are available, there is a plethora of possible combinations. Several authors have compared different approaches for

the adsorption energies of small molecules (hydrocarbons, alcohols, CO<sub>2</sub>, H<sub>2</sub>O) in all-silica zeolites,<sup>[30–34]</sup> as well as protonated and cation-exchanged zeolites,<sup>[21,31,32,34–38]</sup> using values extrapolated from experiment and/or results of higher-level calculations as benchmarks. Without going into the details of the individual studies, the following common findings can be identified:

- XC functionals using the generalised gradient approximation (GGA) without any dispersion correction severely underestimate adsorption energies because the dispersion contribution is missing.
- For alkanes, standard GGA functionals like the Perdew-Burke-Ernzerhof (PBE)<sup>[27]</sup> functional in conjunction with pairwise dispersion corrections, like the D2<sup>[39]</sup> or D3 corrections<sup>[28]</sup> developed by Grimme and co-workers or the TS correction proposed by Tkatchenko and Scheffler,<sup>[40]</sup> have a systematic tendency to overestimate the interaction strength, *i.e.*, they deliver “too negative” adsorption energies.<sup>[31–33,35–37]</sup> While the tendency is generally observed, the degree of overestimation varies across studies. It also depends on the specific adsorbate studied.
- The overestimation is more pronounced when using different flavours of non-local van der Waals density functionals (vdW-DF).<sup>[31–33,35,36,38]</sup>
- Similar trends are observed for other molecules like acetylene, ethylene, and CO<sub>2</sub>.<sup>[21,37]</sup> It is, however, also worth noting that acceptable agreement of PBE-D2 adsorption energies with experimental values was observed for methanol, ethanol, and propanol in MFI-type zeolites,<sup>[32]</sup> and that revPBE-D3 performed very well for H<sub>2</sub>O adsorption energies in CHA-type zeolites.<sup>[34]</sup>
- Calculations in the framework of the random phase approximation (RPA) combine exact (Hartree-Fock) exchange and RPA correlation, which includes information from occupied and virtual orbitals, thus going beyond the approximations made in GGA, meta-GGA, and hybrid XC functionals.<sup>[41]</sup> DFT-based RPA calculations were shown to give fairly good agreement with coupled-cluster benchmark calculations (for small non-periodic model systems)<sup>[37]</sup> or with experimental reference values.<sup>[36]</sup> RPA energies were hence used as benchmark values in a recent comparative study addressing H<sub>2</sub>O adsorption.<sup>[34]</sup>

Studies comparing adsorption energies of larger molecules in zeolites are rarer, and typically include a smaller number of DFT approaches.<sup>[42–44]</sup> In this context, it is worth noting that the validation of DFT calculations dealing with larger molecules faces additional challenges: On the one hand, comparisons to experimental adsorption enthalpies (where available) are much less straightforward for molecules adsorbed from the liquid phase as compared to gases. On the other hand, higher-level reference calculations require larger model systems (supercells of

zeolite unit cells to avoid overlap of a molecule with its images, or large clusters cut out from the zeolite structure), quickly becoming computationally very demanding.

So far, no systematic comparisons of DFT adsorption energies obtained with different approaches have been reported for emerging organic contaminants like pharmaceuticals or personal care products. This study aims to fill this gap, reporting results obtained with a total of 13 dispersion-corrected exchange-correlation (dc-XC) functionals, including five GGA-type functionals and one meta-GGA functional in conjunction with a pairwise D3 correction as well as seven vdW-DF methods. Although a preliminary validation against RPA energies is carried out in the last part for a few adsorption complexes, the main focus is on a comparison of the methods without external reference data. This investigation is structured as follows:

In **Part 1**, adsorption energies are computed for a variety of organic contaminants in two all-silica zeolites (MOR and FAU), with the choice of adsorbents and adsorbates following previous experimental and computational work.<sup>[6,19]</sup> In addition to evaluating the differences in absolute adsorption energies, it is also assessed whether different functionals deliver any appreciable differences in the relative trends.

**Part 2** concentrates on three molecules (acetaminophen – ACA, ibuprofen – IBU, triclosan – TCL) in MOR. For each molecule, different adsorption complexes are considered in order to test to what extent the energetic ordering of different configurations of the same molecule in the same zeolite depends on the chosen approach.

Finally, **Part 3** compares DFT results to adsorption energies from RPA calculations. Due to the computational expense of the RPA calculations, periodic zeolite models are replaced by cluster models in this part, and only the smallest contaminant molecule, acetaminophen, is considered.

It should be emphasised that this work does not attempt to obtain DFT-computed adsorption energies that could be directly compared to any observable quantity. Instead, the key aim is to identify trends within the set of dc-XC functionals. On this basis, some recommendations regarding their probable suitability can be made, allowing to use them with confidence in future studies dealing with the adsorption of emerging organic contaminants or similarly complex organic molecules in zeolites.

## COMPUTATIONAL DETAILS

### Details of DFT calculations

All calculations used the Quickstep electronic structure module within the CP2K code, which uses a Gaussian and plane wave approach.<sup>[45]</sup> For a given contaminant Y in a zeolite, the adsorption energy was calculated as:

$$E_{ads} = E_{DFT, opti}(Zeo + Y) - E_{DFT, sp}(Zeo) - E_{DFT, opti, box}(Y) \quad (1)$$

Here, the first term on the right-hand side corresponds to the DFT total energy obtained from a structure optimisation of Y adsorbed in the pores of the zeolite (adsorption complex), where only the atomic positions of the adsorbate were optimised (see below). The second term is the single-point energy of the guest-free zeolite framework, and the third term corresponds to the energy of the optimised, isolated contaminant molecule.

The DFT calculations in **Part 1** and **2** employed molecularly optimised (MOLOPT) basis sets from the work of VandeVondele and Hutter.<sup>[46]</sup> Both double-zeta short-range basis sets (DZVP-MOLOPT-SR, labelled “DZVP-SR” for brevity in the following) and triple-zeta basis sets (TZVP-MOLOPT, labelled “TZVP” for brevity) were used throughout, as discussed in the Results section. Preliminary tests showed that the use of larger triple-zeta basis sets (TZV2P-MOLOPT, TZV2PX-MOLOPT) resulted in only marginal changes in the adsorption energies that usually remained below 3%. Only the  $\Gamma$  point was used to sample the first Brillouin zone. The plane wave energy cutoff was set to 600 Ry, as preliminary calculations indicated that this value gave well converged adsorption energies (use of an energy cutoff of 800 Ry typically resulted in changes by less than 2%). Goedecker-Teter-Hutter pseudo-potentials developed by Krack were used to represent the core electrons.<sup>[47]</sup> Structure optimisations were considered converged when the following convergence criteria were simultaneously met: Maximal residual force below  $2.5 \cdot 10^{-6}$  Ha bohr<sup>-1</sup> and maximal displacement below  $5 \cdot 10^{-5}$  bohr. For calculations on isolated contaminant molecules, the periodicity was switched off (keyword: PERIODIC: NONE). A wavelet solver was used to solve Poisson’s equation for these non-periodic systems.<sup>[48]</sup> In calculations with non-local vdW-DF functionals, it was found that a Fast Fourier Transform (FFT) cutoff of 400 Ry gave converged results.

### Dispersion-corrected DFT approaches

A total of 13 dc-XC functionals were compared, using otherwise identical settings. They are listed in **Table 1**, which also groups conceptually similar functionals together. While the reader is referred to the references in **Table 1** for details on individual functionals, and to exhaustive

review and benchmarking articles for further information,<sup>[49–53]</sup> these groups are very briefly described in the following:

(1) The five GGA+D3 functionals combine different GGA functionals with the pairwise D3 dispersion correction developed by Grimme and co-workers.<sup>[28]</sup> GGA-type functionals make use of the electron density and its gradient to compute the XC contribution to the total energy. The coefficients to scale the D3 dispersion correction are adjusted depending on the XC functional (see <https://www.chemie.uni-bonn.de/pctc/mulliken-center/software/dft-d3/>).

(2) TPSS-D3 is the only meta-GGA functional combined with the D3 dispersion correction considered in the present work.<sup>[54]</sup> Meta-GGA functionals also employ information on the kinetic energy density to compute the XC contribution, they are computationally moderately more expensive than GGA functionals.

(3) The “van der Waals density functional” (vdW-DF) approach proposed by Dion et al. combines GGA exchange and LDA correlation<sup>[55]</sup> with a non-local correlation contribution, which depends on the electron density and a non-local kernel.<sup>[56]</sup> It is thus designed to incorporate dispersion interactions in a seamless fashion, obviating the need for element-specific dispersion coefficients. As systematic inaccuracies were identified in the original vdW-DF approach, which uses revPBE exchange,<sup>[57]</sup> several combinations with other exchange functionals have been proposed subsequently. In addition to the original implementation, four of these “Non-local vdW-DF1” approaches were considered in this study (**Table 1**).

(4) To improve upon some shortcomings of the vdW-DF1 approach, especially overestimated equilibrium distances and exaggerated attractive dispersion interactions, a modified version of the non-local kernel was implemented by Lee et al. in their vdW-DF2 method.<sup>[58]</sup> A further improved version of vdW-DF2, which uses a revised B86b exchange functional<sup>[59]</sup> instead of PW86 exchange,<sup>[60]</sup> was later proposed by Hamada (rev-vdW-DF2).<sup>[61]</sup>

**Table 1:** Overview of dispersion-corrected DFT approaches used in this work.

Label	Group	Ref.s	Label	Group	Ref.s
PBE-D3	GGA+D3	[27,28]	vdW-DF	Non-local vdW-DF1	[56,57]
revPBE-D3	GGA+D3	[28,57]	vdW-DF-cx	Non-local vdW-DF1	[56,62]
BLYP-D3	GGA+D3	[28,63,64]	vdW-DF-C09	Non-local vdW-DF1	[56,65]
BP86-D3	GGA+D3	[28,59,63]	optPBE-vdW	Non-local vdW-DF1	[56,66]
B97-D3	GGA+D3	[28,39,67]	optB88-vdW	Non-local vdW-DF1	[56,66]
TPSS-D3	meta-GGA+D3	[28,54]	vdW-DF2	Non-local vdW-DF2	[58,60]
			rev-vdW-DF2	Non-local vdW-DF2	[58,59,61]

## RPA and DFT calculations for cluster models

In **Part 3**, single-point RPA calculations were carried out to investigate the interaction of acetaminophen, the smallest organic contaminant molecule considered, with cluster models extracted from the structures of MOR and FAU, taking PBE-D3 optimised structures as starting point, as described in more detail below. The RPA calculations closely followed the approach used in recent work by Stanciakova et al.,<sup>[34]</sup> using the resolution of identity Gaussian and plane wave (RI-GPW) RPA scheme that permits a favourable scaling behaviour with system size.<sup>[68,69]</sup> These calculations employed an energy cutoff of 600 Ry, and 60 Clenshaw-Curtis quadrature points were used in the numerical integration that is required to compute the RI-GPW RPA correlation energy.<sup>[69]</sup> A Schwarz screening threshold of  $10^{-10}$  was used when computing Hartree-Fock exchange. All RPA calculations were performed on non-periodic systems, using the wavelet Poisson solver.<sup>[48]</sup> The adsorption energies were calculated on the basis of the single-point energies obtained for (i) ACA interacting with the zeolite cluster model, (ii) the isolated cluster model, and (iii) isolated ACA.

One set of RPA calculations used correlation-consistent triple-zeta (cc-TZ) Gaussian basis sets, whereas the other set combined cc-TZ basis sets for Si with quadruple-zeta (cc-QZ) basis sets for all other elements (H, C, N, O). Auxiliary RI basis sets were used accordingly. Because the basis set size has a considerable impact on the RPA adsorption energies, adsorption energies were extrapolated to the complete basis set (CBS) using the cubic formula proposed by Helgaker et al.:<sup>[70]</sup>

$$E_{ads,X} = E_{ads,X \rightarrow \infty} + AX^{-3} \quad (2)$$

Here,  $X$  is the cardinal number of the basis set and  $E_{ads,X \rightarrow \infty}$  corresponds to the adsorption energy in the CBS limit. This energy is obtained as intercept of a linear fit with the slope  $A$ . The cardinal number  $X$  equals 3 for the energies obtained with cc-TZ basis sets, and  $X = 3.8$  was assumed for the cc-TZ(Si)/cc-QZ(H,C,N,O) basis sets, as this value reflects the ratio of atoms represented with triple-zeta and quadruple-zeta basis sets (19/18 Si atoms at cc-TZ level, 73/68 H, C, N, and O atoms at cc-QZ level in ACA@MOR/ACA@FAU clusters). To allow for a direct comparison of results obtained with dc-XC functionals to RPA values, the dispersion-corrected DFT calculations were carried out for the same cluster models, using the same basis sets and otherwise analogous settings. Unlike for the periodic DFT calculations, the adsorption energies were also extrapolated to the CBS limit.

## Models of organic contaminants, zeolites, and adsorption complexes

Molecular structures of 21 organic contaminants were taken from earlier work.<sup>[19]</sup> **Table 2** lists these contaminants, including sum formula, molecular weight, and typical applications. The structures had been obtained from the PubChem<sup>[71]</sup> and CheBi<sup>[72]</sup> databases, and were pre-optimised with the DREIDING force field.<sup>[20]</sup> As mentioned above, non-periodic calculations were run for these molecules to avoid artificial interactions between molecules in adjacent simulation cells.

**Table 2:** List of organic contaminants considered in this study. Abbreviations are specified only for those species where the abbreviation is either used in the text or frequently encountered in the literature. The sixth column specifies whether the species were included in Part 1 for MOR and FAU (M+F) or FAU only (F).

	Abbr.	Sum formula	$m_{\text{molar}}$ [g mol <sup>-1</sup> ]	Application	Part 1	Part 2
Acetaminophen	ACA	C <sub>8</sub> H <sub>9</sub> NO <sub>2</sub>	151.17	Analgesic	M+F	M
Atrazine		C <sub>8</sub> H <sub>14</sub> ClN <sub>5</sub>	215.69	Herbicide	M+F	
Caffeine		C <sub>8</sub> H <sub>10</sub> N <sub>4</sub> O <sub>2</sub>	194.19	Stimulant	M+F	
Carbamazepine		C <sub>15</sub> H <sub>12</sub> N <sub>2</sub> O	236.27	Anticonvulsant	F	
<i>N,N</i> -diethyl- <i>meta</i> -toluamide	DEET	C <sub>12</sub> H <sub>17</sub> NO	191.27	Insect repellent	M+F	
Diazepam		C <sub>16</sub> H <sub>13</sub> ClN <sub>2</sub> O	284.75	Anti-anxiety agent	F	
Diclofenac		C <sub>14</sub> H <sub>11</sub> Cl <sub>2</sub> NO <sub>2</sub>	296.15	NSAID	F	
Dilantin (Phenytoin)		C <sub>15</sub> H <sub>12</sub> N <sub>2</sub> O <sub>2</sub>	252.27	Anticonvulsant	F	
Estrone		C <sub>18</sub> H <sub>22</sub> O <sub>2</sub>	270.37	Estrogen	M+F	
Fluoxetine	FLX	C <sub>17</sub> H <sub>18</sub> F <sub>3</sub> NO	309.33	Antidepressant	M+F	
Gemfibrozil		C <sub>15</sub> H <sub>22</sub> O <sub>3</sub>	250.34	Lipid regulator	M+F	
Hydrocodone		C <sub>18</sub> H <sub>21</sub> NO <sub>3</sub>	299.37	Analgesic	F	
Ibuprofen	IBU	C <sub>13</sub> H <sub>18</sub> O <sub>2</sub>	206.29	NSAID	M+F	M
Meprobamate		C <sub>9</sub> H <sub>18</sub> N <sub>2</sub> O <sub>4</sub>	218.25	Anti-anxiety agent	M+F	
Naproxen		C <sub>14</sub> H <sub>14</sub> O <sub>3</sub>	230.26	NSAID	M+F	
Oxybenzone		C <sub>14</sub> H <sub>12</sub> O <sub>3</sub>	228.25	UV absorber	M+F	
Pentoxifylline		C <sub>13</sub> H <sub>18</sub> N <sub>4</sub> O <sub>3</sub>	278.31	Rheological agent	F	
Sulfamethoxazole		C <sub>10</sub> H <sub>11</sub> N <sub>3</sub> O <sub>3</sub> S	253.28	Antibiotic	M+F	
Tri(2-chloroethyl) phosphate	TCEP	C <sub>6</sub> H <sub>12</sub> Cl <sub>3</sub> O <sub>4</sub> P	285.49	Flame retardant	M+F	
Triclosan	TCL	C <sub>12</sub> H <sub>7</sub> Cl <sub>3</sub> O <sub>2</sub>	289.55	Antibacterial agent	M+F	M
Trimethoprim		C <sub>14</sub> H <sub>18</sub> N <sub>4</sub> O <sub>3</sub>	290.32	Antibiotic	M+F	

NSAID = Non-steroidal anti-inflammatory drug

Likewise, the structure models of all-silica MOR and FAU were the same as in earlier work.<sup>[19]</sup> These models were taken from the IZA Database<sup>[2]</sup> and optimised using the force field of Sanders, Leslie, and Catlow (SLC),<sup>[73]</sup> which has been shown to give good agreement with experimental structure data for all-silica zeolites.<sup>[74,75]</sup> Whereas the regular unit cell was used for FAU, a  $1\times1\times3$  supercell was employed for MOR. For the calculations performed in **Part 1**, the initial structures of the adsorption complexes of 15 contaminants in MOR and 21 contaminants in FAU were taken from the previous force field study,<sup>[19]</sup> in which the choice of contaminants had been based on earlier experimental work dealing with MOR- and FAU-type adsorbents.<sup>[6]</sup> Whereas the previous study considered 21 contaminants in both MOR and FAU, six species for which the Monte Carlo insertion into the pores of MOR either failed entirely or was at least problematic were not included in the present work (see **Table 2**). These omissions were motivated by the intention to take a set of adsorption complexes obtained via a consistent computational approach as starting point. In **Part 2**, additional adsorption complexes of ACA, IBU, and TCL adsorbed in MOR were investigated. These configurations were generated via an MD-based annealing approach, using the Forcite module of the DS BIOVIA “Material Studio” suite.<sup>[76]</sup> For each system, two annealing runs, each consisting of 25 heating-cooling cycles within a temperature interval between 300 and 1000 K, were performed, employing the DREIDING force field.<sup>[20]</sup> At the end of each heating-cooling cycle, the structures were optimised with the same force field. For ACA/IBU/TCL, 2/4/4 adsorption complexes were selected from the annealing results. These were studied together with the configurations that were already included in **Part 1**, so a total of 3/5/5 configurations were considered.

In all structure optimisations reported in this article, only the positions of the adsorbed organic contaminants were optimised, and the zeolite structures were held fixed. It is clear that local relaxations of the zeolite framework upon guest molecule adsorption should be taken into account in a comprehensive DFT treatment. In the context of the present work, however, it was deemed preferable to restrict the comparison to host-guest interaction energies and (for selected cases) the positions of adsorbed molecules. Including a relaxation of the zeolite framework would add an additional layer of complexity,<sup>[43]</sup> especially as a considerable dependence of the optimised structural parameters on the chosen DFT approach has been observed in comparative studies of guest-free zeolites.<sup>[77,78]</sup> Several prior benchmarking studies of host-guest interactions in zeolites kept the atomic coordinates of the framework atoms fixed.<sup>[30,37,44]</sup>

The cells of MOR and FAU used in this work are too large to perform periodic RPA calculations with the available computational resources. Therefore, cluster models representing the most significant part of the zeolite framework were employed in the calculations reported in **Part 3**. These cluster models were extracted from the adsorption complexes optimised with the PBE-

D3 functional, considering two different configurations for MOR and one for FAU. The closest part of the zeolite framework was cut out of the periodic structure, resulting in MOR models with 19 T atoms and a FAU model with 18 T atoms. Dangling oxygen atoms were replaced by hydrogen atoms, fixing the Si–H distances to 1.48 Å.<sup>[79]</sup>

## RESULTS

### Part 1: Adsorption of various contaminants in MOR and FAU

The structures of the adsorption complexes (15 species in MOR, 21 species in FAU) and of isolated contaminants were optimised using DZVP-SR basis sets, and the computed adsorption energies are collected in **Table S1.1** (EXCEL spreadsheet **S1**). The adsorption energies were then recomputed using TZVP basis sets, employing the DZVP-SR-optimised structures (**Table S1.2**). A comparison of the  $E_{ads}$  values obtained with the different basis sets reveals appreciable differences, with the DZVP basis sets always delivering larger absolute values (= more negative adsorption energies). Interestingly, the effect of the basis set size varies rather markedly across the set of 13 functionals: For four functionals (BLYP-D3, vdW-DF, optPBE-vdW, vdW-DF2), the average relative deviation, computed over 36 individual values, is on the order of -11 to -12%, whereas it amounts to -19 to -22% for several other functionals including PBE-D3, TPSS-D3, vdW-DF-C09, and rev-vdW-DF2. Due to the important influence of the basis set size, the following discussion considers exclusively the results obtained with the larger TZVP basis sets.

When comparing the adsorption energies computed for a given molecule in one zeolite, the large dependence on the choice of dc-XC functional is immediately apparent. This is illustrated for the smallest and largest contaminant species, acetaminophen (ACA) and fluoxetine (FLX), in **Figure 1**, but a similar overall picture would arise for any of the other contaminants. Starting with ACA@MOR, the most negative adsorption energy value is obtained using the optPBE-vdW functional, with -169 kJ mol<sup>-1</sup>, whereas rev-vdW-DF2 delivers the least negative value of -113 kJ mol<sup>-1</sup>. For ACA@FAU, the same two functionals give the most/least negative adsorption energies of -114 kJ mol<sup>-1</sup> and -76 kJ mol<sup>-1</sup>. The interaction in FAU is significantly weaker than in MOR due to the larger pore size, and hence fewer framework atoms in the distance range of strongest dispersion interactions, as discussed in earlier work.<sup>[19]</sup> For FLX, which interacts much more strongly due to its larger size, optPBE-vdW also results in the most negative adsorption energies, which amount to -265 kJ mol<sup>-1</sup> and -214 kJ mol<sup>-1</sup> for adsorption in MOR and FAU, respectively. By contrast, the rev-vdW-DF2 functional predicts adsorption energies of -166 kJ mol<sup>-1</sup> and -139 kJ mol<sup>-1</sup>. Across the set of energy values, optPBE-vdW

delivers the strongest interaction for all but three zeolite-contaminant combinations, where optB88-vdW and in one case also BP86-D3 give more negative values. On the other side of the spectrum, rev-vdW-DF2 gives the least negative  $E_{ads}$  values for all but three combinations, where different functionals using the D3 dispersion correction (PBE-D3, revPBE-D3, B97-D3, TPSS-D3) result in less negative values. The differences between the maximal and minimal  $E_{ads}$  values for a given combination fall between 33 and 99 kJ mol<sup>-1</sup>, or between 30 and 40% in relative terms.

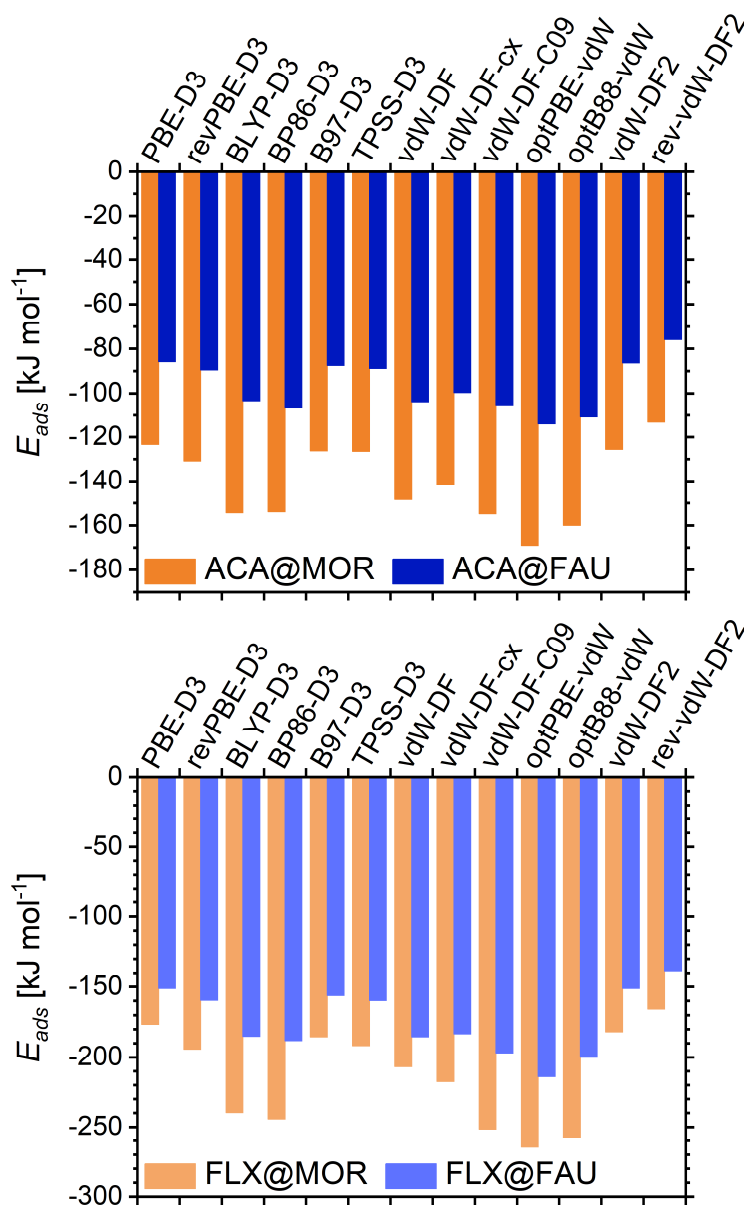


**Figure 1:** Adsorption energies computed for ACA (top) and FLX (bottom) in MOR (orange columns) and FAU (blue columns) using different dc-XC functionals.

On the basis of the results presented above, it can be clearly stated that the choice of dc-XC functional has a very large impact on the absolute values of the adsorption energies. However, it will often be more relevant to identify qualitative trends, rather than computing accurate absolute values, especially as it is difficult to benchmark the latter against experimental data. Such qualitative trends could be important, for example, in a search for zeolite adsorbents having a particularly strong affinity towards a given contaminant. It is therefore important to assess to what extent the trends predicted by different functionals differ. For illustrative purposes, the adsorption energies obtained with the BP86-D3, TPSS-D3, optPBE-vdW, and rev-vdW-DF2 functionals are plotted against the PBE-D3 energies in **Figure 2**. It has to be emphasised that the use of PBE-D3 as reference is made for convenience here, and is not meant to imply that the PBE-D3 energies are expected to be of superior accuracy. In principle, any other functional could be taken as reference.

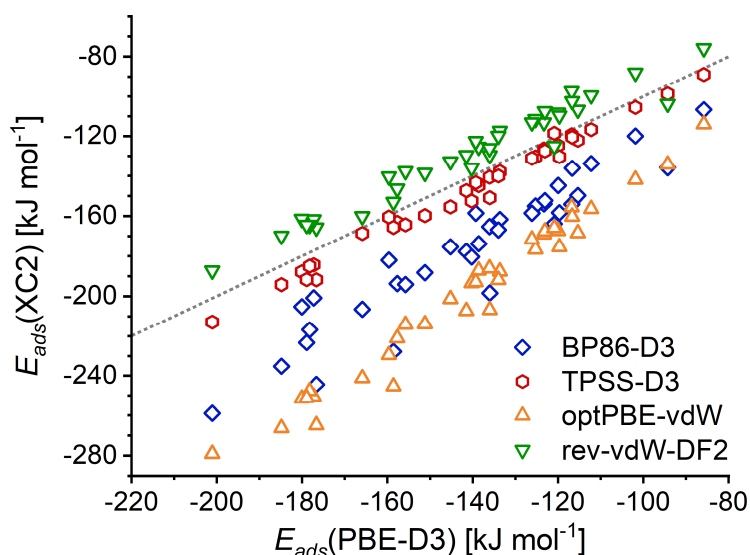


**Figure 2:** Adsorption energies for the whole set of contaminants adsorbed in MOR and FAU, computed with different dc-XC functionals and plotted against the PBE-D3 adsorption energies. The dotted line indicates a slope of 1.

**Figure 2** shows essentially linear trends for all four functionals, with only a few outliers that appear to be more prominent for BP86-D3 and rev-vdW-DF2 compared to TPSS-D3 and optPBE-vdW. Whereas the adsorption energies obtained with TPSS-D3 and rev-vdW-DF2 fall slightly below and above the grey line that represents a perfect linear correlation with a slope of 1, BP86-D3 and especially optPBE-vdW deliver systematically more negative adsorption energies, as could be expected from the discussion above. For a more quantitative assessment, it is useful to calculate least-square linear regression lines of the form

$E_{ads}(XC2) = m_{12} \cdot E_{ads}(XC1)$ , where  $XC1 = \text{PBE-D3}$  and  $XC2 = \text{another dc-XC functional}$  (the intercept is set to zero because no offset should occur in the limit of no interaction). For the four functionals, the following slopes and squared correlation coefficients  $R^2$  were obtained: BP86-D3:  $m_{12} = 1.252$ ,  $R^2 = 0.892$ ; TPSS-D3:  $m_{12} = 1.047$ ,  $R^2 = 0.987$ ; optPBE-vdW:  $m_{12} = 1.413$ ,  $R^2 = 0.973$ ; rev-vdW-DF2:  $m_{12} = 0.918$ ,  $R^2 = 0.955$ .

In order to evaluate the similarities and differences among the functionals in a more comprehensive fashion, regression lines across the dataset were computed, using all combinations of  $XC1$  and  $XC2$ . The results are collected in **Figure 3**, where the top right half reports the slopes of the linear regression lines and the bottom left half gives the respective squared correlation coefficients. Redundant slope values that could be computed as  $m_{21} = 1/m_{12}$  (with the same  $R^2$ ) are omitted. On the basis of these results, the XC functionals can be grouped as follows:

- Three of the five GGA+D3 functionals, PBE/revPBE/B97-D3, as well as the meta-GGA TPSS-D3 functional give adsorption energies of very similar magnitude ( $m_{12}$  values ranging from 0.97 to 1.05) and the results are highly correlated with each other ( $R^2 > 0.97$ ).
- The other two GGA+D3 functionals, BLYP-D3 and BP86-D3, deliver adsorption energies that are, on average, 23 to 25% more negative than those obtained using PBE-D3. While the results obtained with these two functionals are highly correlated, correlations with other functionals are less prominent, with most  $R^2$  values being smaller than 0.95.
- Adsorption energies that are 20 to 40% more negative than the PBE-D3 energies are obtained with the functionals belonging to the vdW-DF1 group. They exhibit a varying degree of correlation with each other and with other functionals.
- vdW-DF2 gives rather similar results as PBE-D3, with  $m_{12}$  amounting to 1.02 and a squared correlation coefficient of 0.96. rev-vdW-DF2 is the only functional for which the slope  $m_{12}$  for  $XC1 = \text{PBE-D3}$  is smaller than one, with the adsorption energies being about 8% less negative. Apart from a very strong correlation with vdW-DF2, correlations with other functionals fall in a range of  $0.93 < R^2 < 0.97$ .

Altogether, the results from this part show that use of different functionals results in pronounced differences in the magnitude of absolute adsorption energies. On the other hand, all functionals deliver very similar qualitative trends, with even the smallest squared correlation coefficient amounting to 0.84, and all except four  $R^2$  values being larger than 0.9.

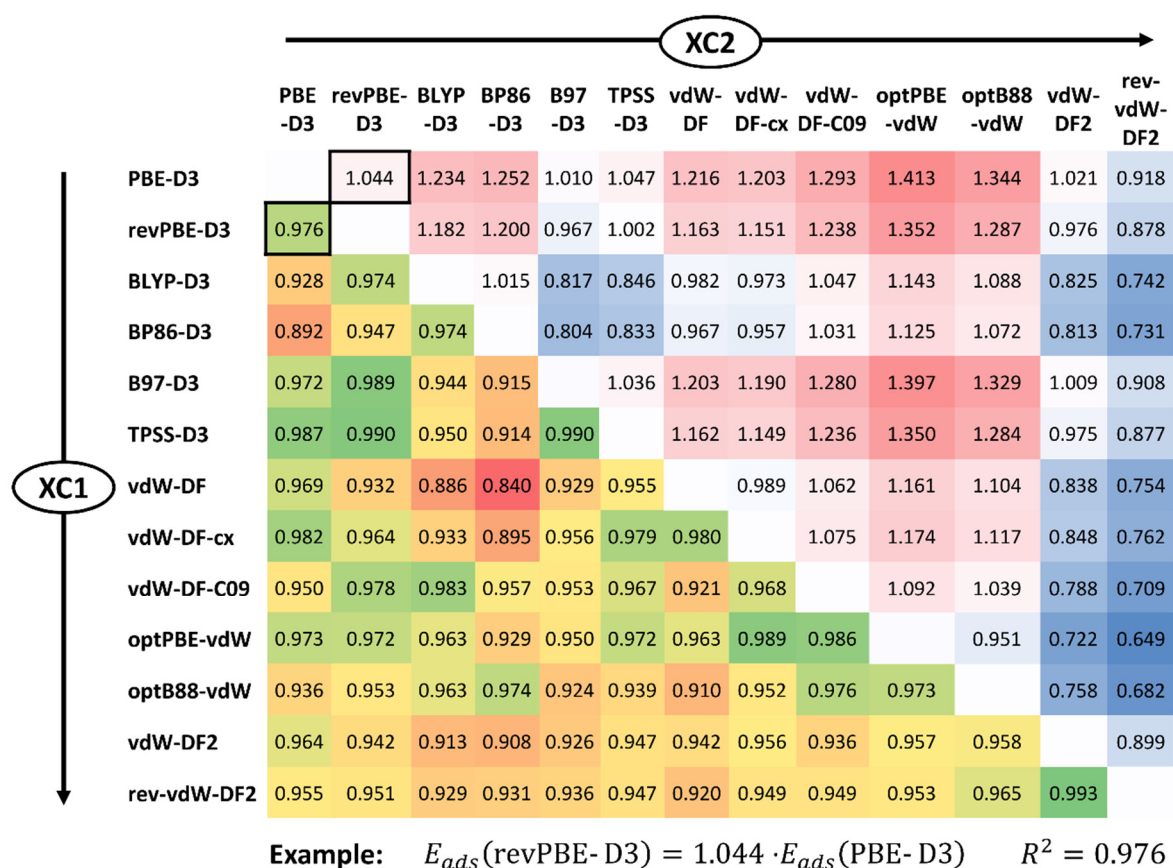


**Figure 3: Top right:** Slopes  $m_{12}$  of linear regressions obtained on the basis of adsorption energies computed with exchange-correlation functionals XC1 and XC2. **Bottom left:** Squared correlation coefficients  $R^2$  for combinations of functionals. The values for the example XC1 = PBE-D3, XC2 = revPBE-D3 are highlighted with black frames.

## Part 2: Different adsorption configurations of ACA, IBU, and TCL in MOR

Having shown the large impact of the choice of functional on the total adsorption energy, it is now interesting to assess to what extent the energetic ordering of different configurations of the same molecule in one zeolite is affected, both in terms of adsorption energies and structures of the adsorption complexes. For this purpose, the investigation focussed on three organic contaminants, acetaminophen, ibuprofen, and triclosan, which differ considerably in terms of adsorption energies and conformational degrees of freedom. **Figure 4** shows the adsorption configurations of ACA@MOR that were included in the calculations (IBU@MOR and TCL@MOR configurations are shown in Table **S2.0** of EXCEL spreadsheet **S2**). In each case, Config1 corresponds to the configuration that was already included in **Part 1**, and the other configurations (2/4/4 for ACA/IBU/TCL) were generated using preliminary annealing simulations with the DREIDING force field.

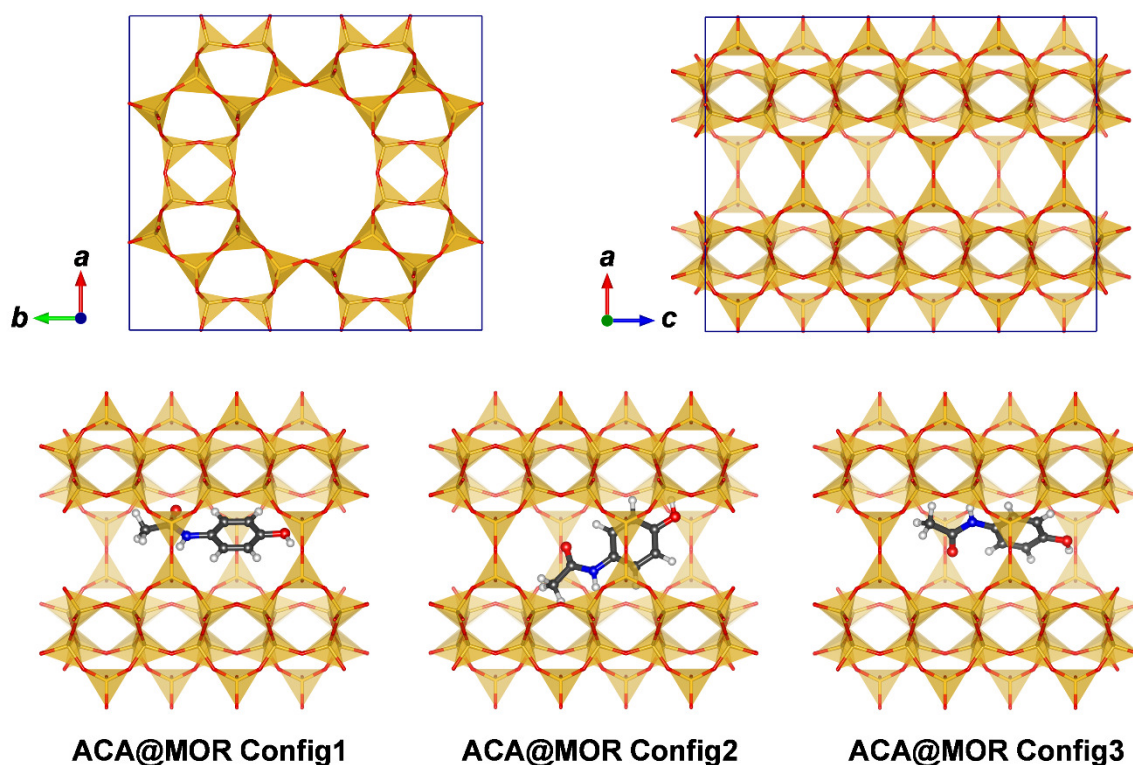


**Figure 4:** **Top:** Visualisation of the unit cell of MOR in projections along [001] and [010]. The 12-membered ring channels run along the *c* direction. **Bottom:** Adsorption configurations of acetaminophen in the channels of MOR. Only the surrounding portion of the channel is shown.

Unlike in **Part 1**, the structures of the adsorption complexes (and of free contaminant molecules) were optimised using TZVP basis sets. For the Config1 cases, these “TZVP/TZVP” adsorption energies can be directly compared to adsorption energies obtained from TZVP single-point calculations on DZVP-SR-optimised structures (“TZVP/DZVP-SR”). These results are collected in the lower part of **Table S2.1**. The differences between TZVP/TZVP and TZVP/DZVP-SR adsorption energies remain below 5 kJ mol<sup>-1</sup> (in absolute terms), with the mean of absolute errors across the three contaminants not exceeding 2.3 kJ mol<sup>-1</sup>, and remaining below 1.0 kJ mol<sup>-1</sup> for 8 of the 13 functionals. As the total adsorption energies fall between -110 and -250 kJ mol<sup>-1</sup>, such changes can be considered negligible.

**Table S2.1** also contains the adsorption energies obtained for all 13 configurations with the different XC functionals. An analysis of correlations analogous to that of **Part 1** gives similar results to those discussed above (**Table S2.2**), since it is dominated by the absolute adsorption energy values. In order to assess the energetic ordering of different configurations, the energy differences  $\Delta E_{ads}$  with respect to the Config1 models (relative energies) were calculated (**Table S2.3**). **Figure 5** shows the  $\Delta E_{ads}$  values obtained with the PBE-D3, B97-D3, vdW-DF, vdW-DF2, and rev-vdW-DF2 functionals. For ACA@MOR Config2, IBU@MOR Config3, and

IBU@MOR Config5, all functionals give  $\Delta E_{ads}$  values close to zero, but the sign differs, in other words, different functionals disagree on whether the configurations are slightly more or less stable than the respective Config1. Even though a similarly small  $\Delta E_{ads}$  value is calculated for ACA@MOR Config3 (in other words, all three ACA@MOR configurations are very close together in energy), very consistent results are obtained with all shown functionals except B97-D3. For the remaining configurations, where the  $\Delta E_{ads}$  values are significantly larger, PBE-D3, vdW-DF2, and rev-vdW-DF2 deliver results within a few  $\text{kJ mol}^{-1}$  of each other, as well as giving the same energetic orderings (e.g., for TCL@MOR: Config1 – Config2 – Config3 – Config5 – Config4). B97-D3 and vdW-DF both show larger absolute deviations, as well as predicting a different ordering of the configurations.

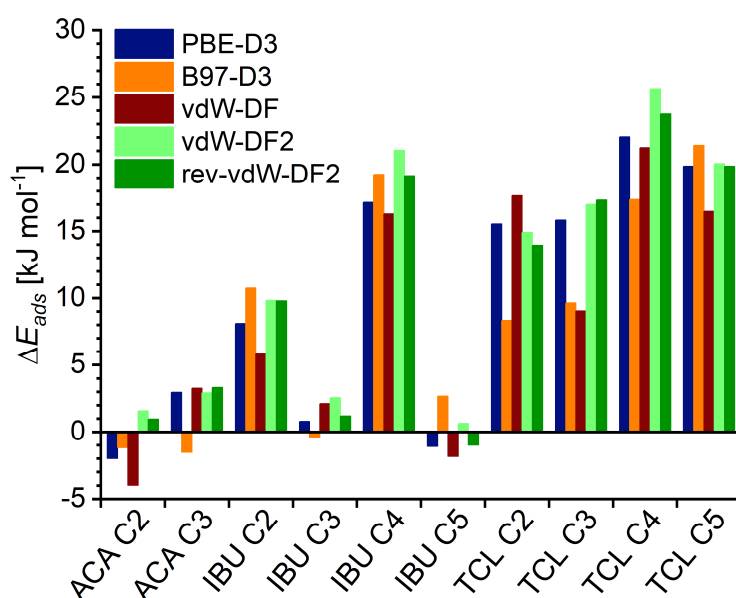


**Figure 5:** Relative energy  $\Delta E_{ads}$  for different configurations of ACA/IBU/TCL@MOR (reference: Config1, for which  $\Delta E_{ads} = 0$ ).

While the absolute values obtained with different functionals fall in similar ranges, the relative deviations in individual values may be considerable, especially for small  $\Delta E_{ads}$  values. Hence, the usefulness of a linear fit through the origin is limited. On the other hand, an analysis of the correlations between  $\Delta E_{ads}$  values can still be insightful. The resulting  $R^2$  values are compiled in Table S2.4. Among the (meta-)GGA+D3 functionals, PBE-D3, revPBE-D3, and TPSS-D3 give fairly highly correlated results. Interestingly, the  $\Delta E_{ads}$  values obtained with three functionals from the vdW-DF1 group (vdW-DF-C09, optPBE-vdW, optB88-vdW) and with vdW-DF2 and rev-vdW-DF2 are highly correlated with the PBE/revPBE/TPSS-D3 results, and with each other. A less prominent, but still significant correlation is observed for vdW-DF and vdW-

DF-cx. In contrast,  $\Delta E_{ads}$  values computed with the BLYP-D3, BP86-D3, and B97-D3 functionals are relatively poorly correlated with those calculated with other functionals.

Looking beyond adsorption energies, it is also insightful to assess to what extent the choice of functional affects the equilibrium structure of the adsorbed contaminant (as noted above, structural parameters of the zeolite framework were held fixed in all calculations). While a detailed analysis could make use of various intermolecular quantities (bond lengths, bond angles, dihedral angles) as well as distances to framework atoms, it would quickly become very cumbersome, given the number of configurations and dc-XC functionals considered. As it is the main aim of the present analysis to determine how similar or different the configurations obtained with different functionals are, a less refined approach was used: In this approach, the PBE-D3 optimised structures were taken as reference, and the distance vectors  $\vec{v}_i$  between the positions of a given atom  $i$  in the structure optimised with another functional and its position in the PBE-D3 structure were computed. The average positional deviation  $dev$  was then calculated over all  $N$  atoms as  $dev = \frac{1}{N} \sum_i^N |\vec{v}_i|$ .<sup>[80]</sup> As in **Part 1**, the use of PBE-D3 coordinates as reference is arbitrary, as coordinates optimised with any other functional could equally well be used. However, PBE-D3 appears as an appropriate choice as numerous other dc-XC functionals give relatively similar  $\Delta E_{ads}$  values.

The deviations for individual configurations are shown in **Figure 6** (coordinates are compiled in **Tables S2.6 to S2.8**, and numerical values of  $dev$  are given in **Table S2.9**). The average  $\overline{dev}$  values calculated over all 13 configurations are also included in that figure. Closest agreement with the PBE-D3 structures is found for optPBE-vdW, followed by vdW-DF2, rev-vdW-DF2, and optB88-vdW. For all these functionals, the majority of the individual  $dev$  values remain below 0.15 Å, indicating only relatively modest differences in the position of the adsorbed molecules. This agrees with the correlation in the  $\Delta E_{ads}$  values found above. The remaining three vdW-DF1 functionals form a second tier, where a significant number of individual configurations have  $dev$  values above 0.2 Å, but below 0.3 Å, indicating reasonable similarity with the PBE-D3 structures. Despite using the same dispersion correction as PBE-D3, all of the other GGA+D3 functionals and TPSS-D3 result in at least one individual configuration having a  $dev$  value above 0.3 Å. Among these, the overall deviation from the PBE-D3 structures is less pronounced for revPBE-D3 and TPSS-D3, which also deliver relatively similar  $\Delta E_{ads}$  values. The other three functionals give very different equilibrium structures than PBE-D3 in several instances, with the most pronounced differences occurring for some IBU@MOR configurations optimised with the BP86-D3 functional.

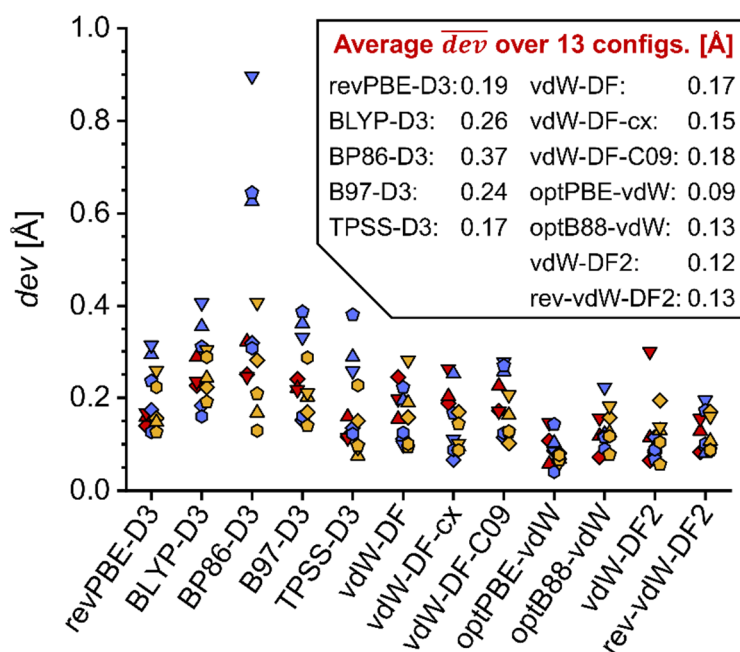


**Figure 6:** Average deviation  $dev$  in atomic coordinates of adsorbed ACA/IBU/TCL molecules with respect to PBE-D3 reference coordinates. Individual deviations are represented with symbols, using the following scheme: ACA@MOR = red symbols, IBU@MOR = blue symbols, TCL@MOR = yellow symbols. Config1 = diamonds, Config2 = upright triangles, Config3 = inverted triangles, Config4 = pentagons, Config5 = hexagons. To avoid symbol overlap, symbols for ACA and TCL are slightly shifted to the left and right, respectively. Averages over all configurations are given in the inset.

All three molecules considered in this part contain OH groups. Hydrogen bonds between these groups and framework oxygen atoms may make a significant contribution to the host-guest interaction. It is therefore interesting to evaluate to what extent different functionals differ in the description of these bonds in terms of hydrogen bond distances and angles. To determine whether hydrogen bonds are present or not, the configurations optimised with the PBE-D3 functional were analysed, considering all cases as hydrogen-bonded where the  $d(\text{H}_{\text{OH}} \cdots \text{O}_{\text{fw}})$  distance is smaller than 2.5 Å. On this basis, hydrogen bonds were found in 7 out of 13 configurations: ACA@MOR Config2 and 3, IBU@MOR Config1 and 5, TCL@MOR Config2, 3, and 4. Even though there are a few instances where functionals other than PBE-D3 give distances slightly below 2.5 Å for additional configurations, the use of the PBE-D3 structures as reference point is consistent with the approach used above for the overall deviations in coordinates. In almost all cases, the shortest  $d(\text{H}_{\text{OH}} \cdots \text{O}_{\text{fw}})$  contacts are formed to the same framework oxygen atom in configurations optimised with different functionals, with the few exceptions corresponding to configurations having rather large  $\overline{dev}$  values (*e.g.*, TCL@MOR Config3 optimised with BP86-D3 and BLYP-D3). When looking at the individual  $d(\text{H}_{\text{OH}} \cdots \text{O}_{\text{fw}})$  distances, listed in **Table S2.10**, some scatter is evident, with the difference between the shortest and longest distance as obtained with different functionals varying between 0.13 and

0.31 Å. However, there are no clearly discernible trends in the sense that some functionals deliver systematically longer distances than others. As a consequence, a calculation of the average over all seven configurations results in relatively similar values, which fall in a range from 2.31 to 2.38 Å. Corresponding observations can be made for the hydrogen bond angles.

### Part 3: Comparison to RPA calculations for cluster models

Due to the immense computational overhead of periodic RPA calculations for systems of the size of MOR or FAU, these calculations were performed for two cluster models of ACA@MOR adsorption complexes studied in **Part 2**, as well as a cluster model of the ACA@FAU complex studied in **Part 1**. For ACA@MOR, Config1 and Config3 were chosen for the following reasons: First, the ACA molecules are displaced from the channel centre, interacting primarily with one side of the channel wall. Therefore, a relatively small cluster model should be able to capture the largest part of the host-guest interactions. In contrast, the ACA molecule in Config2 lies across the channel, interacting with both sides, so a much larger model would be required (**Figure 4**). Second, although DFT calculations deliver very similar adsorption energies for both configurations, Config3 contains a  $\text{H}_{\text{OH}} \cdots \text{O}_{\text{fw}}$  hydrogen bond, whereas Config1 does not. All cluster models were cut out from the structures optimised using the PBE-D3 functional and TZVP (for MOR) or DZVP-SR (for FAU) basis sets. They are visualised in **Figure 7**.

Because full structure optimisations using RPA are computationally too demanding, only single-point calculations were carried out. To evaluate all methods on an equal footing, the DFT adsorption energies were computed for the same cluster models. In order to test whether the use of PBE-D3 optimised structures, rather than a full optimisation with the respective approach, affects the results, single-point calculations for periodic structures were carried out with the 13 functionals, using the PBE-D3 structures optimised in **Part 1** (ACA@FAU) and **Part 2** (ACA@MOR). To also assess the influence of the basis sets, separate calculations were carried out with the cc-TZ and mixed cc-TZ/cc-QZ basis sets, which made a recalculation of the energies of the guest-free zeolites and isolated ACA necessary. The results are summarised in **Table S3.1**. Starting with the PBE-D3 results, use of cc-TZ basis sets gives slightly more negative adsorption energies than use of TZVP basis sets, whereas the  $E_{\text{ads}}$  values obtained with cc-TZ/cc-QZ basis sets are essentially identical to the TZVP energies. For the other functionals, the use of PBE-D3 structures and different basis sets also leads to only modest changes in the computed energies, with the maximal positive/negative deviations from the TZVP values amounting to +3.6/-3.7 kJ mol<sup>-1</sup> for cc-TZ basis sets, and +6.6/-2.5 kJ mol<sup>-1</sup> for the mixed cc-TZ/cc-QZ basis sets. Altogether, the trends in adsorption energies across the set of functionals that were established in **Part 1** are not affected by the use of

different basis sets, and by employing PBE-D3 optimised structures. These results validate the outlined strategy of carrying out single-point calculations on clusters cut out from the PBE-D3 structures with different dc-XC functionals and comparing them to reference values obtained from RPA calculations on the same clusters.

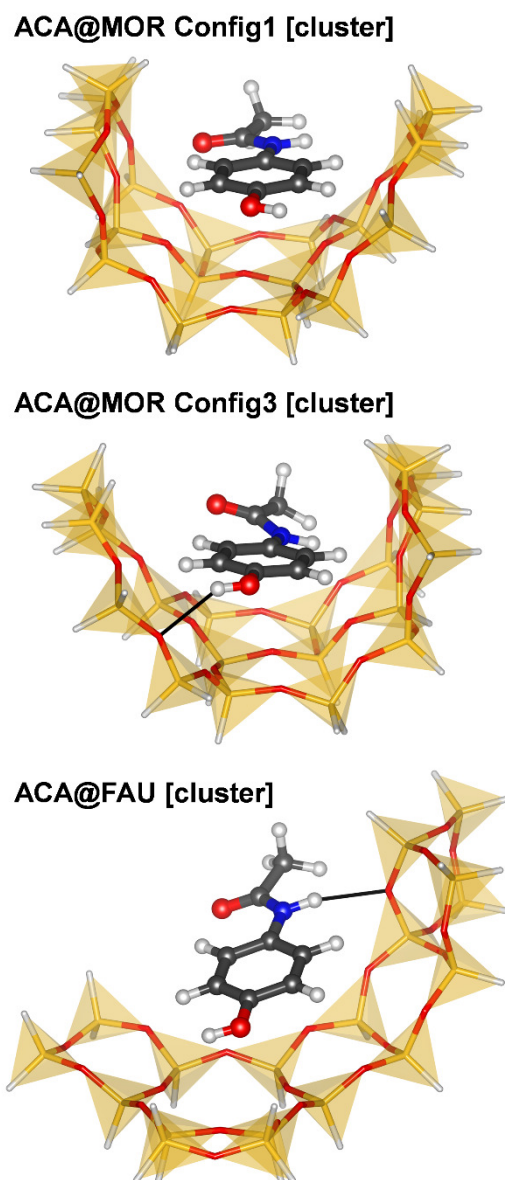


**Figure 7:** Cluster models used in calculations of **Part 3**. Thin black lines indicate hydrogen bonds.

The RPA and DFT adsorption energies computed for the cluster models shown in **Figure 7** are compiled in **Table S3.2**.  $E_{ads}$  values obtained directly from the calculations using cc-TZ and cc-TZ/cc-QZ basis sets as well as CBS-extrapolated values are given in that table. First

of all, it is worth noting that the CBS extrapolation has a much larger impact for the RPA energies in comparison to the energies calculated with dc-XC functionals: For the RPA results, the energies obtained with mixed cc-TZ/cc-QZ basis sets are -12 to -17 kJ mol<sup>-1</sup> more negative than the CBS-extrapolated values (cc-TZ: -24 to -35 kJ mol<sup>-1</sup>), whereas the corresponding differences among the DFT results amount to -1 to -6 kJ mol<sup>-1</sup>. Second, it is useful to compare the DFT adsorption energies obtained for the cluster models to the corresponding values computed for periodic structures (**Table S3.1**). Due to the missing contribution of long-range interactions with framework atoms at larger distances from the ACA molecule, the  $E_{ads}$  values calculated for clusters are distinctly less negative. The differences to the results computed for periodic models range from 18 to 49 kJ mol<sup>-1</sup>, corresponding to 22 to 33% in relative terms. The relative differences are fairly similar across the set of dc-XC functionals, indicating that the contribution from longer-range interactions that is missing when using cluster models is not strongly dependent on the functional.

The key question to be addressed in this part is the agreement between adsorption energies computed with dc-XC functionals and RPA reference values. To facilitate this analysis, the differences  $\Delta E_{ads} = E_{ads}(XC1) - E_{ads}(RPA)$  are visualised in **Figure 8**. It is apparent that identical trends are observed for all three configurations, with the three  $\Delta E_{ads}$  values of any particular dc-XC functional being identical in sign and similar in magnitude. Therefore, the mean of signed errors (MSE), included in **Table S3.2**, can be employed to measure the agreement with the RPA results, resulting in the following observations:

- The PBE-D3 functional delivers near-perfect agreement with RPA. Although it can be anticipated that the very small MSE of -0.8 kJ mol<sup>-1</sup> is a result of fortuitous error cancellations (see **Discussion**), it has to be noted that the MSE is significantly smaller than for any other functional, corresponding to about 1/5 of the second-smallest value.
- revPBE-D3, B97-D3, TPSS-D3, and vdW-DF2 exhibit an only modest tendency to deliver more negative adsorption energies than RPA, with MSE values between -4.2 and -5.5 kJ mol<sup>-1</sup>. This tendency is somewhat more pronounced for vdW-DF and vdW-DF-cx (MSE: -7.4/-8.7 kJ mol<sup>-1</sup>).
- BLYP-D3, BP86-D3, vdW-DF-C09, optPBE-vdW, and optB88-vdW result in a massive overestimation of the interaction strength, with MSEs on the order of -20 to -30 kJ mol<sup>-1</sup>. On a relative scale, the adsorption energies are 25 to 40% more negative than the RPA values.
- Finally, rev-vdW-DF2 is the only functional that delivers less negative adsorption energies than RPA. The MSE is modest, amounting to 4.4 kJ mol<sup>-1</sup>.

It is clear that some caution has to be exercised in the interpretation of these results, as will be discussed in more detail below. However, it is also obvious that the observed trends are systematic, and that the qualitative and quantitative differences among different functionals are considerable.

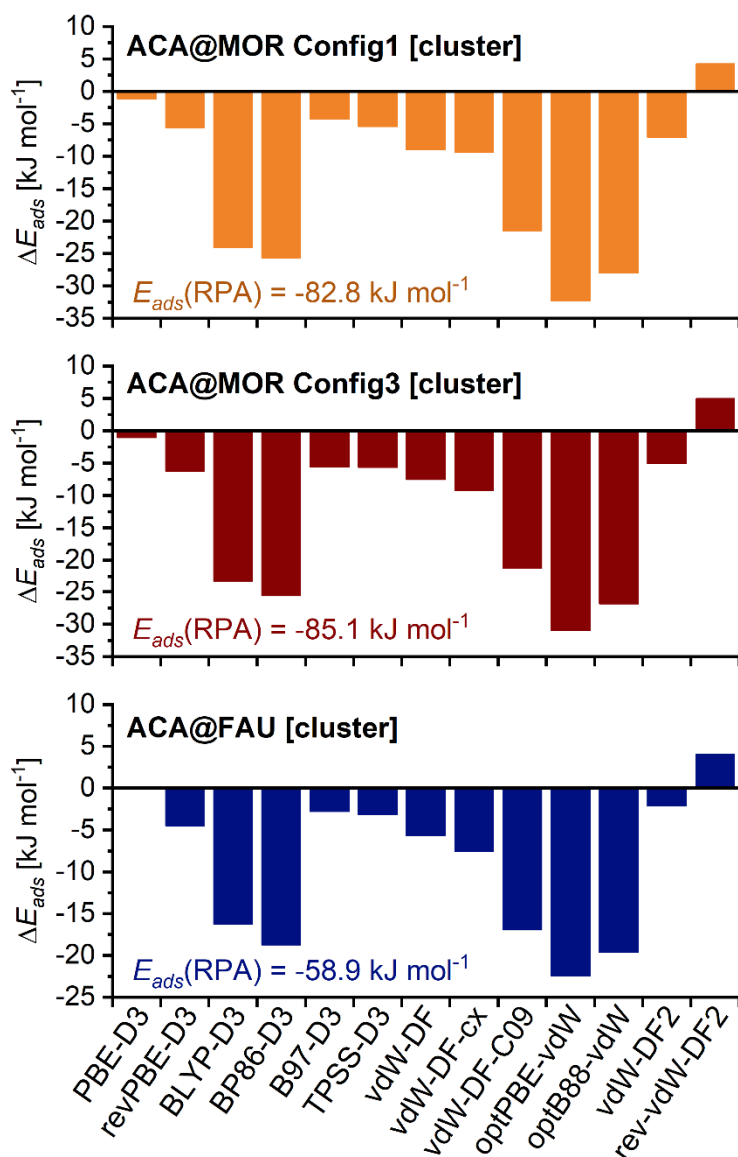


**Figure 8:** Difference  $\Delta E_{ads}$  between CBS-extrapolated adsorption energies calculated using dc-XC functionals and RPA reference values for the three cluster models shown in **Figure 7**. RPA reference values are given as insets.

## DISCUSSION

### Effect of basis set size and optimisation strategy

The results obtained in **Parts 1** and **2** show very clearly that the use of DZVP-SR basis sets results in systematically more negative adsorption energies compared to TZVP basis sets. The differences among results obtained with different basis sets vary considerably, depending on the dc-XC functional used and the adsorbate, indicating that there is no simple way to extrapolate from smaller to larger basis sets. Reassuringly, the comparison of adsorption energies obtained with TZVP MOLOPT basis sets to cc-TZ/cc-QZ energies showed only modest quantitative differences, indicating that TZVP basis sets may constitute a good balance between accuracy and computational cost, especially for periodic systems. It is, however, also clear that benchmark calculations should, wherever feasible, go beyond triple-zeta basis set quality.

The comparison of results from **Part 1**, where the structures were optimised using DZVP-SR basis sets, and **Part 2**, where a full optimisation using TZVP basis sets was performed, showed that the optimisation with the larger basis sets had only a marginal influence on the resulting adsorption energies. From the viewpoint of an efficient use of computational resources, it seems thus attractive to routinely combine optimisations with smaller basis sets and adsorption energy calculations using larger basis sets. This strategy could also be employed for AIMD simulations, where a few snapshots from a trajectory might be extracted for a recalculation of energies with larger basis sets. Nevertheless, it is clear that there may also be cases where a full optimisation with triple-zeta (or larger) basis sets can be desirable, *e.g.*, when aiming at a detailed analysis of the equilibrium structure.

Finally, it was shown in **Part 3** that the use of PBE-D3 structures in the calculation of adsorption energies with different dc-XC functionals had only a modest influence on the results when compared to full optimisations using the respective functional (which is maybe a bit surprising, given the rather large variations in the equilibrium positions of the adsorbed molecules observed in some cases in **Part 2**). Therefore, it may be sufficient to pre-optimize the structures with one functional prior to calculations of the adsorption energies using a larger number of functionals when aiming to get a first overview. In this way, the set of approaches could be narrowed down to the most promising ones in order to avoid computationally demanding optimisations with dc-XC functionals exhibiting systematic errors.

## Comparing different dc-XC functionals: Quantitative differences, qualitative similarities

All three parts of this work corroborated a massive dependence of the adsorption energies on the choice of dc-XC functional, with quantitative deviations that frequently amount to several 10 per cent in relative terms. These variations are essentially independent of the choice of basis sets or the optimisation strategy. Hence, it is clear that any study that is aimed at an even semi-quantitative computation of adsorption energies for organic contaminants (or other sizeable organic molecules) in zeolites will have to pay considerable attention to the use of an appropriate DFT approach. On the other hand, the results of **Part 1** showed that qualitative trends are not strongly affected by the dc-XC functional. Therefore, the results of DFT-based investigations that are primarily aimed at the identification of zeolite-guest combinations exhibiting strong interaction should be fairly insensitive to the choice of approach. Although the occurrence of some outliers in **Figure 2** serves as a reminder that caution must be exercised in individual cases, the overall findings indicate that the identification of zeolite adsorbents having a high affinity towards a given contaminant should, in the majority of cases, not depend strongly on the dc-XC functional, at least among the 13 functionals tested.

Compared to the calculation of adsorption energies for different combinations of zeolites and contaminants, the energetic ordering of different adsorption configurations for the same zeolite-contaminant combination constitutes a more intricate problem. Frequently, the energy differences among different configurations are on the order of a few  $\text{kJ mol}^{-1}$ , and it is clear that none of the dispersion-corrected DFT approaches considered could deliver an accuracy that would allow to determine the energetic ordering with certainty. For those configurations that are not too close in energy, the majority of functionals give qualitatively and quantitatively similar results with regard to the relative energies of different configurations. It is noteworthy that there is no one-to-one correspondence between absolute adsorption energies and relative energies of different configurations: For example, optPBE-vdW delivers adsorption energies that are 40 to 70  $\text{kJ mol}^{-1}$  more negative than those obtained with PBE-D3 for ACA, IBU, and TCL adsorbed in MOR, but the relative energies of different configurations computed with these two functionals agree to within 1  $\text{kJ mol}^{-1}$ .

The comparison of the adsorption complexes optimised with different dc-XC functionals showed that numerous functionals give fairly similar results. Specifically, three of the vdW-DF1 approaches and both vdW-DF2 approaches delivered atomic positions that are very close to those obtained with PBE-D3. The agreement in the coordinates is rather striking when considering that the adsorption energies computed with these methods vary considerably: For example, the smallest deviation in coordinates from PBE-D3 was found for optPBE-vdW, which, as discussed in the preceding paragraph, gives much more negative adsorption energies. Rather surprisingly, substantial deviations were apparent among the GGA+D3

functionals, despite the consistent derivation of the dispersion correction term. This indicates that the exchange-correlation contribution has an important impact on the equilibrium position of the guest molecule, despite the dominant influence of dispersion interactions on the total interaction strength. Altogether, it can be concluded that functionals giving similar adsorption energies do not necessarily deliver similar equilibrium structures, and vice versa. More comprehensive benchmarking studies against higher-level data should therefore take both interaction energies and structural properties into account.

### **Choosing a suitable DFT approach**

Although the results have shown that qualitative predictions of trends in adsorption energies will not be heavily affected by the choice of dc-XC functional, it is clear that one will usually strive to employ an approach that gives reasonably “accurate” adsorption energies. In this context, the term “accurate” is not meant to reflect the “chemical accuracy” that is often the goal in high-level benchmarking studies, but to reflect a performance that is largely free from systematic over- or underestimations. Compared to gas-phase adsorption, where sophisticated approaches to derive adsorption energies from experimentally measured adsorption enthalpies have been developed,<sup>[81]</sup> the situation is more complex for species adsorbed from the liquid phase, and a direct comparison to experimental values does not, at present, appear as a feasible strategy to gauge the performance of DFT approaches. To obtain higher-level reference values, RPA calculations were carried out for a few cluster models. Clearly, this benchmarking remained preliminary for various reasons: First, only one organic molecule and only a few configurations of that molecule were considered in the RPA calculations; future work should include a larger set of species and configurations. Second, the use of cluster models means that the contribution of long-range interactions is absent both in the RPA energies and in the DFT values computed for the same models. If some dc-XC functionals exhibited systematic errors in the description of these longer-ranger interactions, they would go unnoticed in cluster calculations. Third, it was noted that the CBS extrapolation had a massive impact on the RPA reference values. Although the strategy employed here has been successfully used in previous work,<sup>[34]</sup> explicit RPA calculations with larger basis sets should be done in the future, at least for some reference systems of limited size.

Having noted these caveats, it appears nevertheless reasonable to rank the dc-XC functionals in terms of their agreement with the RPA results. Several of these functionals deliver much more negative adsorption energies than RPA, agreeing with the previously established trend that dispersion-corrected DFT approaches tend to overestimate the interaction strength in adsorption complexes. On this basis, BLYP-D3, BP86-D3, vdW-DF-C09, optPBE-vdW, and

optB88-vdW can certainly be discarded. While the relative deviations found for vdW-DF and vdW-DF-cx are smaller, they are large enough to rule them out as well. This leaves the functionals PBE-D3, revPBE-D3, B97-D3, TPSS-D3, vdW-DF2 and rev-vdW-DF2 as those that agree to (approximately) within 5 kJ mol<sup>-1</sup> with the RPA results. Among the four functionals including a D3 dispersion correction, PBE-D3 agrees most closely with the RPA reference values, and even though it is reasonable to expect that the excellent numerical agreement is partially due to error cancellation, this functional can be recommended as a robust choice for studies of sizeable organic contaminants in zeolites. This result is at variance with several studies of smaller molecules in zeolites, where PBE-D3 was typically found to overestimate the interaction strength systematically (albeit not as prominently as many functionals from the non-local vdW-DF1 family).<sup>[31,33–38]</sup> The origins of this discrepancy cannot be resolved in the context of the present work, and future investigations appear warranted. A second aspect that has to be considered in future studies that include an optimisation of the zeolite framework concerns the description of the framework: Although it was found that PBE-D3 delivers very good agreement with experimental unit cell parameters of all-silica zeolites, it was also noted that this good performance partly stems from error cancellation, as an overestimation of Si–O bond lengths is compensated by an underestimation of Si–O–Si angles.<sup>[77]</sup> Although these shortcomings may not play a critical role in many instances, they should be kept in mind for a balanced assessment.

Like the revPBE-D3, B97-D3, and TPSS-D3 functionals, vdW-DF2 also exhibits a modest tendency to deliver too negative adsorption energies with respect to RPA reference values. This finding aligns with earlier studies on small molecules in zeolites, where a more pronounced overestimation of the interaction strength by vdW-DF2 as compared to PBE-D3 was observed. Besides, the vdW-DF2 functional was found to give a poor description of the structure of guest-free all-silica zeolites, tending to overestimate both unit cell parameters and Si–O bond lengths rather drastically.<sup>[77]</sup> The rev-vdW-DF2 functional performed significantly better, showing similar tendencies as PBE-D3 outlined above. Moreover, rev-vdW-DF2 also performed robustly for different groups of weakly bound solids in a wide-ranging benchmarking study, indicating that it may not suffer from systematic errors that impede the transferability of many other dc-XC functionals.<sup>[53]</sup> Focussing on adsorption energies, rev-vdW-DF2 is remarkable as it is the only functional delivering less negative values than RPA, maintaining acceptable quantitative agreement. The tendency to predict weaker interaction than other dc-XC functionals is also observed across the large set of zeolite-guest combinations included in **Part 1**. If it is taken for granted that most dc-XC functionals tend to overestimate the interaction strength of adsorption complexes in zeolites, rev-vdW-DF2 logically emerges as an attractive choice as this tendency is least pronounced, or possibly altogether absent. Although previous studies employing this functional to compute adsorption energies in zeolites are lacking,

Vlaisavljevich et al. used rev-vdW-DF2 – together with several other functionals – in a study of CO<sub>2</sub>, CH<sub>4</sub>, and H<sub>2</sub>O adsorption in metal-organic frameworks (MOFs) with open metal sites.<sup>[82]</sup> They observed excellent agreement with experimental  $E_{ads}$  values (derived from adsorption enthalpies) and metal-guest equilibrium distances (obtained from in-situ neutron diffraction). The good performance for MOFs with positively polarised open metal sites could imply that rev-vdW-DF2 is also suitable for adsorption in cationic zeolites, where a reasonable representation of the interaction with the cations will be crucial. In addition, it is worth noting that another benchmarking study addressing H<sub>2</sub> adsorption on graphene reported very good agreement of rev-vdW-DF2 results with experimental reference values, with no systematic tendency to overestimate the interaction strength.<sup>[83]</sup>

## CONCLUDING REMARKS

Calculations for a set of 21 organic contaminants in two all-silica zeolites that employed 13 dispersion-corrected DFT approaches revealed significant quantitative differences in the computed adsorption energies. Qualitative trends, however, were not so heavily affected, indicating that different dc-XC functionals should give similar answers when attempting to identify zeolites having a high affinity towards a given contaminant. This is particularly noteworthy when considering that the contaminants possess a variety of different functional groups. Even when comparing different configurations of one molecule in the same zeolite, several functionals gave very similar results, both in terms of relative energies and equilibrium positions of the adsorbed organics. Interestingly, no systematic deviations among different groups of functionals could be identified; for example, some vdW-DF1 functionals showed much closer agreement with PBE-D3 results than some GGA+D3 functionals. In quantitative terms, rev-vdW-DF2 and PBE-D3 were the two functionals giving the least negative adsorption energies. These functionals also gave excellent (PBE-D3) and good (rev-vdW-DF2) agreement with RPA calculations for a few cluster models. Altogether, it appears safe to conclude that PBE-D3 and rev-vdW-DF2 should be suitable choices for future DFT studies of organic contaminants or related functional organic molecules in zeolites. This is especially relevant as these two functionals are well applicable for zeolites with large unit cells, where the use of more demanding approaches (e.g., hybrid functionals) will incur a significant computational overhead. These functionals should also provide a useful starting point for the validation of FF parameters, which could then, in turn, be employed in MC or MD simulations to investigate the adsorption and diffusion of large organics in zeolites.

Clearly, the present study can be expanded in various directions. First of all, efforts should be undertaken to obtain benchmark energy values against which the DFT results can be

compared in a more comprehensive manner, either from experiment or from high-level calculations. If such values become available, the trends identified here could provide some indications regarding the likely performance of different functionals, potentially allowing to discard some of the 13 dc-XC functionals included here and to consider some others instead. Second, further work should include temperature effects, and potentially also consider the choice of an appropriate reference state that would, ultimately allow the prediction of adsorption enthalpies for species adsorbed from aqueous solution. Third, adsorption-induced deformations of the zeolite framework should be accounted for. Finally, protonated or cation-exchanged can be more attractive than all-silica zeolites for some applications involving the adsorption of functional organic molecules. Future DFT studies of these systems, which have a more heterogeneous charge distribution, would require a separate validation. For example, it is well known that the PBE-D3 functional results in systematic errors for cationic zeolites,<sup>[35]</sup> and it would be very interesting to evaluate whether rev-vdW-DF2 performs better for these materials.

## Acknowledgments

Funding by the Deutsche Forschungsgemeinschaft (German Research Foundation, DFG) through a Heisenberg scholarship (project no. 455871835) is gratefully acknowledged. This work was supported by the North-German Supercomputing Alliance (HLRN). The author is indebted to Dr. Filip Formalik (Northwestern University) for a careful and critical reading of a draft version of this manuscript.

## Supporting Information

EXCEL files `S1.xlsx`, `S2.xlsx` and `S3.xlsx` compile the results of **Part 1**, **2**, and **3**. The optimised structures from **Part 1** and **2** are included in ZIP archives `S1_Contaminants.zip`, `S1_MOR.zip`, `S1_FAU.zip`, and `S2_MOR_Configs.zip`. The cluster models used in **Part 3** as well as sample input files and log files of RPA calculations are included in the ZIP archive `S3_Cluster_models_RPA.zip`.

## References

- [1] N. Jiang, R. Shang, S. G. J. Heijman, L. C. Rietveld, *Water Res.* **2018**, *144*, 145–161.
- [2] C. Baerlocher, L. B. McCusker, <http://www.iza-structure.org/databases/>, **2021**.
- [3] I. Braschi, S. Blasioli, L. Gigli, C. E. Gessa, A. Alberti, A. Martucci, *J. Hazard. Mater.* **2010**, *178*, 218–225.
- [4] S. Fukahori, T. Fujiwara, R. Ito, N. Funamizu, *Desalination* **2011**, *275*, 237–242.
- [5] A. Martucci, L. Pasti, N. Marchetti, A. Cavazzini, F. Dondi, A. Alberti, *Microporous Mesoporous Mater.* **2012**, *148*, 174–183.
- [6] A. Rossner, S. A. Snyder, D. R. U. Knappe, *Water Res.* **2009**, *43*, 3787–3796.
- [7] D. J. De Ridder, J. Q. J. C. Verberk, S. G. J. Heijman, G. L. Amy, J. C. Van Dijk, *Separ. Purif. Technol.* **2012**, *89*, 71–77.
- [8] L. Pasti, E. Sarti, A. Cavazzini, N. Marchetti, F. Dondi, A. Martucci, *J. Separ. Sci.* **2013**, *36*, 1604–1611.
- [9] A. H. Yonli, I. Batonneau-Gener, J. Koulidiati, *J. Hazard. Mater.* **2012**, *203–204*, 357–362.
- [10] M. Van den Bergh, A. Krajnc, S. Voorspoels, S. R. Tavares, S. Mullens, I. Beurroies, G. Maurin, G. Mali, D. E. De Vos, *Angew. Chem. - Int. Ed.* **2020**, *59*, 14086–14090.
- [11] P. Horcajada, C. Márquez-Alvarez, A. Rámila, J. Pérez-Pariente, M. Vallet-Regí, *Solid State Sci.* **2006**, *8*, 1459–1465.
- [12] D. G. Fatouros, D. Douroumis, V. Nikolakis, S. Ntais, A. M. Moschovi, V. Trivedi, B. Khima, M. Roldo, H. Nazar, P. A. Cox, *J. Mater. Chem.* **2011**, *21*, 7789–7794.
- [13] M. Spanakis, N. Bouropoulos, D. Theodoropoulos, L. Sygellou, S. Ewart, A. M. Moschovi, A. Siokou, I. Niopas, K. Kachrimanis, V. Nikolakis, P. A. Cox, I. S. Vizirianakis, D. G. Fatouros, *Nanomedicine Nanotechnology, Biol. Med.* **2014**, *10*, 197–205.
- [14] A. J. Wise, J. S. Sefy, E. Barbu, A. J. O'Malley, S. M. van der Merwe, P. A. Cox, *J. Control. Release* **2020**, *327*, 140–149.
- [15] R. Fantini, G. Vezzadini, A. Zambon, E. Ferrari, F. Di Renzo, M. Fabbiani, R. Arletti, *Microporous Mesoporous Mater.* **2021**, *328*, 111478.
- [16] A. Thiel, K. Muffler, N. Tippkötter, K. Suck, U. Sohling, S. M. Hruschka, R. Ulber, *J. Chem. Technol. Biotechnol.* **2015**, *90*, 1999–2006.
- [17] P. Baile, E. Fernández, L. Vidal, A. Canals, *Analyst* **2019**, *144*, 366–387.
- [18] S. Leon, G. Sastre, *J. Phys. Chem. C* **2022**, *126*, 2078–2087.
- [19] M. Fischer, *Mater. Adv.* **2020**, *1*, 86–98.
- [20] S. L. Mayo, B. D. Olafson, W. A. Goddard, *J. Phys. Chem.* **1990**, *94*, 8897–8909.
- [21] H. Fang, P. Kamakoti, J. Zang, S. Cundy, C. Paur, P. I. Ravikovitch, D. S. Sholl, *J. Phys. Chem. C* **2012**, *116*, 10692–10701.

- [22] M. Fischer, R. G. Bell, *J. Phys. Chem. C* **2012**, *116*, 26449–26463.
- [23] P. Bai, M. Tsapatsis, J. I. Siepmann, *J. Phys. Chem. C* **2013**, *117*, 24375–24387.
- [24] B. Vujić, A. P. Lyubartsev, *Model. Simul. Mater. Sci. Eng.* **2016**, *24*, 045002.
- [25] R. Xiong, S. I. Sandler, D. G. Vlachos, *J. Phys. Chem. C* **2011**, *115*, 18659–18669.
- [26] N. Jiang, M. Erdős, O. A. Moutos, R. Shang, T. J. H. Vlugt, S. G. J. Heijman, L. C. Rietveld, *Chem. Eng. J.* **2020**, *389*, 123968.
- [27] J. P. Perdew, K. Burke, M. Ernzerhof, *Phys. Rev. Lett.* **1996**, *77*, 3865–3868.
- [28] S. Grimme, J. Antony, S. Ehrlich, H. Krieg, *J. Chem. Phys.* **2010**, *132*, 154104.
- [29] D. Schwalbe-Koda, R. Gómez-Bombarelli, *J. Chem. Phys.* **2021**, *154*, 174109.
- [30] F. Labat, A. H. Fuchs, C. Adamo, *J. Phys. Chem. Lett.* **2010**, *1*, 763–768.
- [31] F. Göttl, A. Grüneis, T. Bučko, J. Hafner, *J. Chem. Phys.* **2012**, *137*, 114111.
- [32] C. Chiu, G. N. Vayssilov, A. Genest, A. Borgna, N. Rösch, *J. Comput. Chem.* **2014**, *35*, 809–819.
- [33] H. Fang, R. Awati, S. E. Boulfelfel, P. I. Ravikovitch, D. S. Sholl, *J. Phys. Chem. C* **2018**, *122*, 12880–12891.
- [34] K. Stanciakova, J. N. Louwen, B. M. Weckhuysen, R. E. Bulo, F. Göttl, *J. Phys. Chem. C* **2021**, *125*, 20261–20274.
- [35] F. Göttl, J. Hafner, *J. Chem. Phys.* **2011**, *134*, 064102.
- [36] F. Göttl, J. Hafner, *Microporous Mesoporous Mater.* **2013**, *166*, 176–184.
- [37] J. Klimeš, D. P. Tew, *J. Chem. Phys.* **2019**, *151*, 234108.
- [38] F. R. Rehak, G. Piccini, M. Alessio, J. Sauer, *Phys. Chem. Chem. Phys.* **2020**, *22*, 7577–7585.
- [39] S. Grimme, *J. Comput. Chem.* **2006**, *27*, 1787–1799.
- [40] A. Tkatchenko, M. Scheffler, *Phys. Rev. Lett.* **2009**, *102*, 073005.
- [41] X. Ren, P. Rinke, C. Joas, M. Scheffler, *J. Mater. Sci.* **2012**, *47*, 7447–7471.
- [42] I. Khalil, H. Jabraoui, G. Maurin, S. Lebègue, M. Badawi, K. Thomas, F. Maugé, *J. Phys. Chem. C* **2018**, *122*, 26419–26429.
- [43] T. J. Goncalves, P. N. Plessow, F. Studt, *ChemCatChem* **2019**, *11*, 4368–4376.
- [44] P. N. Plessow, F. Studt, *J. Phys. Chem. Lett.* **2020**, *11*, 4305–4310.
- [45] T. D. Kühne, M. Iannuzzi, M. Del Ben, V. V. Rybkin, P. Seewald, F. Stein, T. Laino, R. Z. Khaliullin, O. Schütt, F. Schiffmann, D. Golze, J. Wilhelm, S. Chulkov, M. H. Bani-Hashemian, V. Weber, U. Borštnik, M. TAILLEFUMIER, A. S. Jakobovits, A. Lazzaro, H. Pabst, T. Müller, R. Schade, M. Guidon, S. Andermatt, N. Holmberg, G. K. Schenter, A. Hehn, A. Bussy, F. Belleflamme, G. Tabacchi, A. Glöß, M. Lass, I. Bethune, C. J. Mundy, C. Plessl, M. Watkins, J. VandeVondele, M. Krack, J. Hutter, *J. Chem. Phys.* **2020**, *152*, 194103.

- [46] J. VandeVondele, J. Hutter, *J. Chem. Phys.* **2007**, *127*, 114105.
- [47] M. Krack, *Theor. Chem. Acc.* **2005**, *114*, 145–152.
- [48] L. Genovese, T. Deutsch, A. Neelov, S. Goedecker, G. Beylkin, *J. Chem. Phys.* **2006**, *125*, 074105.
- [49] S. Grimme, A. Hansen, J. G. Brandenburg, C. Bannwarth, *Chem. Rev.* **2016**, *116*, 5105–5154.
- [50] J. Hermann, R. A. DiStasio, A. Tkatchenko, *Chem. Rev.* **2017**, *117*, 4714–4758.
- [51] F. Tran, J. Stelzl, P. Blaha, *J. Chem. Phys.* **2016**, *144*, 204120.
- [52] N. Mardirossian, M. Head-Gordon, *Mol. Phys.* **2017**, *115*, 2315–2372.
- [53] F. Tran, L. Kalantari, B. Traoré, X. Rocquefelte, P. Blaha, *Phys. Rev. Mater.* **2019**, *3*, 063602.
- [54] J. Tao, J. P. Perdew, V. N. Staroverov, G. E. Scuseria, *Phys. Rev. Lett.* **2003**, *91*, 146401.
- [55] J. P. Perdew, Y. Wang, *Phys. Rev. B* **1992**, *45*, 13244–13249.
- [56] M. Dion, H. Rydberg, E. Schröder, D. C. Langreth, B. I. Lundqvist, *Phys. Rev. Lett.* **2004**, *92*, 246401.
- [57] Y. Zhang, W. Yang, *Phys. Rev. Lett.* **1998**, *80*, 890.
- [58] K. Lee, É. D. Murray, L. Kong, B. I. Lundqvist, D. C. Langreth, *Phys. Rev. B* **2010**, *82*, 081101.
- [59] J. P. Perdew, *Phys. Rev. B* **1986**, *33*, 8822–8824.
- [60] J. P. Perdew, Y. Wang, *Phys. Rev. B* **1986**, *33*, 8800–8802.
- [61] I. Hamada, *Phys. Rev. B* **2014**, *89*, 121103.
- [62] K. Berland, P. Hyldgaard, *Phys. Rev. B* **2014**, *89*, 035412.
- [63] A. D. Becke, *Phys. Rev. A* **1988**, *38*, 3098–3100.
- [64] C. Lee, W. Yang, R. G. Parr, *Phys. Rev. B* **1988**, *37*, 785–789.
- [65] V. R. Cooper, *Phys. Rev. B* **2010**, *81*, 161104.
- [66] J. Klimeš, D. R. Bowler, A. Michaelides, *J. Phys. Condens. Matter* **2010**, *22*, 022201.
- [67] A. D. Becke, *J. Chem. Phys.* **1997**, *107*, 8554.
- [68] M. Del Ben, J. Hutter, J. VandeVondele, *J. Chem. Theory Comput.* **2013**, *9*, 2654–2671.
- [69] M. Del Ben, O. Schütt, T. Wentz, P. Messmer, J. Hutter, J. VandeVondele, *Comput. Phys. Commun.* **2015**, *187*, 120–129.
- [70] T. Helgaker, W. Klopper, H. Koch, J. Noga, *J. Chem. Phys.* **1997**, *106*, 9639–9646.

- [71] S. Kim, J. Chen, T. Cheng, A. Gindulyte, J. He, S. He, Q. Li, B. A. Shoemaker, P. A. Thiessen, B. Yu, L. Zaslavsky, J. Zhang, E. E. Bolton, *Nucleic Acids Res.* **2019**, *47*, D1102–D1109.
- [72] J. Hastings, G. Owen, A. Dekker, M. Ennis, N. Kale, V. Muthukrishnan, S. Turner, N. Swainston, P. Mendes, C. Steinbeck, *Nucleic Acids Res.* **2016**, *44*, D1214–D1219.
- [73] M. J. Sanders, M. Leslie, C. R. A. Catlow, *J. Chem. Soc. Chem. Commun.* **1984**, 1271–1273.
- [74] A. F. Combariza, D. A. Gomez, G. Sastre, *Chem. Soc. Rev.* **2013**, *42*, 114–127.
- [75] M. Fischer, F. O. Evers, F. Formalik, A. Olejniczak, *Theor. Chem. Acc.* **2016**, *135*, 257.
- [76] D. S. BIOVIA, *BIOVIA Materials Studio 2019*, DS Biovia, **2019**.
- [77] M. Fischer, W. J. Kim, M. Badawi, S. Lebègue, *J. Chem. Phys.* **2019**, *150*, 094102.
- [78] A. Hoffman, M. Deluca, D. Hibbitts, *J. Phys. Chem. C* **2019**, *123*, 6572–6585.
- [79] R. D. Johnson (Editor), “NIST Computational Chemistry Comparison and Benchmark Database,” can be found under <http://cccbdb.nist.gov/>, **2020**.
- [80] M. Fischer, *Z. Kristallogr. - Cryst. Mater.* **2015**, *230*, 325–336.
- [81] G. Piccini, M. Alessio, J. Sauer, Y. Zhi, Y. Liu, R. Kolvenbach, A. Jentys, J. A. Lercher, *J. Phys. Chem. C* **2015**, *119*, 6128–6137.
- [82] B. Vlaisavljevich, J. Huck, Z. Hulvey, K. Lee, J. A. Mason, J. B. Neaton, J. R. Long, C. M. Brown, D. Alfè, A. Michaelides, B. Smit, *J. Phys. Chem. A* **2017**, *121*, 4139–4151.
- [83] I. Cabria, M. J. López, J. A. Alonso, *J. Chem. Phys.* **2017**, *146*, 214104.